Article

Partial Power Processing Based Converter for Electric Vehicle Fast Charging Stations

Jon Anzola *, Iosu Aizpuru and Asier Arruti

Department of Electronics and Computer Science, Mondragon Unibertsitatea, 20120 Hernani, Spain;
iaizpuru@mondragon.edu (I.A.); aarruti@mondragon.edu (A.A.)
* Correspondence: janzola@mondragon.edu

Abstract: This paper focuses on the design of a charging unit for an electric vehicle fast charging station. With this purpose, in first place, different solutions that exist for fast charging stations are described through a brief introduction. Then, partial power processing architectures are introduced and proposed as attractive strategies to improve the performance of this type of applications. Furthermore, through a series of simulations, it is observed that partial power processing based converters obtain reduced processed power ratio and efficiency results compared to conventional full power converters. So, with the aim of verifying the conclusions obtained through the simulations, two downscaled prototypes are assembled and tested. Finally, it is concluded that, in case galvanic isolation is not required for the charging unit converter, partial power converters are smaller and more efficient alternatives than conventional full power converters.

Keywords: electric vehicle; fast charging stations; partial power processing; partial power converters; series connected converter; dual active bridge

1. Introduction

Through the last years, the automotive market is showing a big interest on the inclusion of the electric vehicle (EV). Indeed, due to its efficient performance and reduced greenhouse emissions, the EV is turning into a real alternative to conventional combustion based vehicles. This can be confirmed by analyzing its shelling data, which increases year by year [1]. However, one of the main disadvantages of EVs is their low autonomy, which can reach up to 550 km [2]. In order to solve this problem, there exist 2 main solutions: invest on technologies that can extend the capacity of the energy storage system (ESS) or build an extensive and solid EV charging stations grid. The first solution is usually high time consuming, since experimental tests of different battery technologies require long periods. However, the second solution is much faster and if the charging stations are correctly located, the driving rage anxiety of the EV user can be reduced [3].

According to ref. [4], there exist different concepts of EV charging stations: exchanging vehicle's battery [5], contactless inductive coupled chargers [6] and conductive coupled chargers. Regarding conductive coupled chargers, this type of chargers are the most popular solution for EV charging and currently, inside Europe there exists a great number of charging points based on this technology [7]. When it comes to the different types of conductive EV charging stations, they can be divided by their power level. On the one hand, up to 10 kW AC charging stations can be found. Usually, this type of charging structures are located where people spend great part of the day, for example: at home or at work. On the other hand, DC wise, two main groups exist: fast charging stations (between 20 kW and 120 kW) and extreme fast charging stations (higher than 120 kW). Due to the high peak power values, the charging times can be reduced up to 15 min [8], which makes the EV more attractive to the customer.

Concerning conductive EV fast charging stations, Figure 1 shows different implemented structures. As it can be observed, in all the solutions, fast charging stations are connected to a medium voltage AC grid and, then, the voltage level is reduced and rectified. Finally, a DC-DC power converter is implemented to charge each EV at the station. However, the location of galvanic isolation and the way to step down the voltage are managed in different ways. For example, in Figure 1a, the voltage is reduced by a line frequency transformer and then rectified by an AC-DC converter. This way, a common DC bus is obtained from which the rest of the DC-DC individual charging units are connected. In the case of Figure 1b,c, the line frequency transformer is avoided by implementing solid-state transformers on the AC-DC rectifier or on the DC-DC converter.

(**a**)

(**b**)

(**c**)
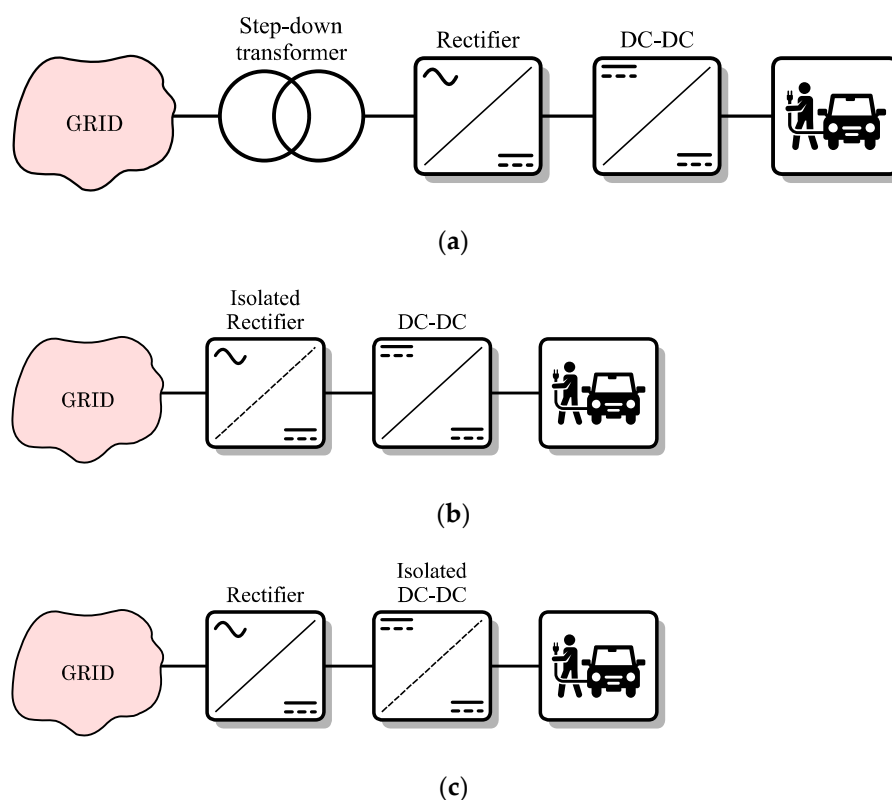
Figure 1. Simplified single-wire diagram of different electric vehicle (EV) fast charging station solutions. (**a**) Galvanic isolation is provided by a line frequency transformer; (**b**) Galvanic isolation is provided by the AC-DC rectifier; (**c**) Galvanic isolation is provided by the DC-DC charging unit.

This paper will focus on the design of the DC-DC converter, which is connected between a common DC bus and the ESS of the EV. Since the concerned converter is required to process great power values, its size, cost and performance are key factors that must be optimized through its design. Due to this, recent literature around EV fast charging applications presents advance architectures based on partial power processing (PPP). This type of architectures aim to reduce the power processed by the converter, achieving reduced size and more efficient converters. Due to the mentioned benefits, their applications are diverse. For example, authors from [9–11] propose PPP based architectures for photovoltaic (PV) systems, whereas [12,13] suggest PPP solutions for ESS applications. There, the concerned converter is designed to control the power flow between the source and the load. Moreover, through [14,15], authors present DC windfarms based on PPP technology. Apart from that, with the aim of achieving current balancing of series connected elements, refs. [16–19] present PPP architectures for applications where there exist series connected elements. Last but not least, when it comes to EV fast charging applications authors from [8,20,21] propose PPP based charging units. There, the authors implement a

unidirectional topology such as the phase shifted full bridge and they show that the PPP solution achieves converter rating reduction and efficiency improvements compared to its full power processing (FPP) version. Therefore, it is concluded that PPP based converters are very suitable for the concerned application.

Finally, in relation to the normative around EV charging systems, at present, the great majority of countries oblige to implement isolated DC-DC converters. This fact affects negatively to PPP architectures, which can never ensure galvanic isolation (unless an extra transformer is added). Nevertheless, through the last years, the normative around EV charging stations is suffering considerable changes. For example, the requirement of galvanic isolation is on discussion and, in some cases, the application of non-isolated supply equipment is allowed for EV charging [22]. To be more precise, the only countries that are included at the corrigendum of the normative are the United States and Canada. Although there are only two countries that permit non-isolated solutions, they can be considered as worldwide references that can encourage others to follow the same route.

Bearing all this mind, the present paper aims to design a PPP based DC-DC charging unit for an EV fast charging station and compare its performance against a conventional full power converter (FPC). Through the concerned comparison, special interest will be shown on the temperature evolution of the PPC prototype. Indeed, these results help to understand the real benefit of processing less power and to have a bigger picture when carrying out the design of a partial power converter. To achieve this, in first place, Section 2 introduces and describes the concept of PPP. Then, Section 3 presents the case studio to simulate and the followed design procedure. Next, Section 4 and Section 5 present the obtained results from the simulations and the experimental tests, respectively. Finally, Section 6 and Section 7 detail the obtained conclusions through the paper and the proposed future lines.

2. Basis of Partial Power Processing

As its name indicates, a power converter based on the PPP concept only processes a reduced percentage of the total power that goes from the source to the load. As example, Figure 2 shows the power flow of a converter based on FPP and a converter based on PPP. On the one hand, as it can be observed in Figure 2a, the FPP converter is designed to process the 100% of the power consumed by the load, generating a given quantity of losses. On the other hand, Figure 2b shows the PPP concept, which is based on achieving a reduction of the power processed by the converter. This way, the losses generated by the power converter are reduced, as well as its size. Furthermore, maintaining the same efficiency for the power converter, the global efficiency of the system increases.

(a)

(b)
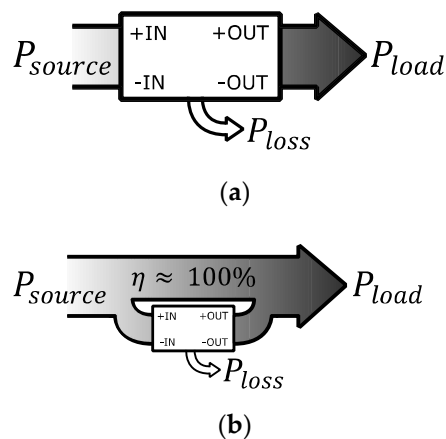
Figure 2. Power flow diagram. (**a**) FPP; (**b**) PPP.

The literature around PPP presents different strategies that achieve a reduction of the total power processed by the converter [23]. On one side, differential power converters (DPC) can be found, whose main objective is to correct current unbalances between series connected elements. On the other side, there are the partial power converters (PPC), which control the power flow between a source and a load with different voltage and current values. Concerning PPCs, different types of architectures can be found in the literature. Figure 3 presents two examples for step-down applications [12,21,24,25]. The architecture from Figure 3a is referred as "Input-Series-Output-Parallel" (ISOP) and the one from Figure 3b is defined as "Input-Parallel-Output-Series" (IPOS). In order to compare the architectures shown in Figure 3, the first step is to calculate the processed active power ratio (K_{pr}) of the converter at each one. For that purpose, the architecture from Figure 3a is taken as an example. Firstly, Kirchhoff's laws are applied on the architecture, obtaining expressions Equations (1) and (2). In addition, the efficiency of the system is defined as shown in Equation (3).

$$V_{source} - V_{in} = V_{load} \tag{1}$$

$$I_{source} + I_{pc} = I_{load} \tag{2}$$

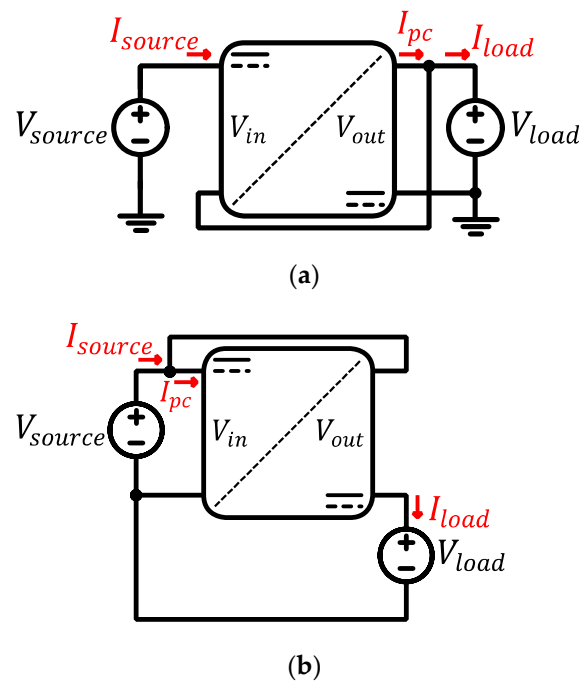$$\eta_{system} = \frac{V_{load} \cdot I_{load}}{V_{source} \cdot I_{source}} \tag{3}$$

(**a**)

(**b**)

Figure 3. Step-down PPC architectures. (**a**) ISOP; (**b**) IPOS.

Then, the K_{pr} is defined as the division between the processed power by the converter and the source's power Equation (4).

$$K_{pr} = \frac{P_{conv}}{P_{source}} = \frac{V_{out} \cdot I_{pc}}{V_{source} \cdot I_{source}} \tag{4}$$

Applying Equations (1)–(4), it is possible to obtain the K_{pr} curve in function of the static voltage gain $\left(G_V = \frac{V_{load}}{V_{source}}\right)$, see Equation (5).

$$K_{pr} = \eta_{system} - G_V \tag{5}$$

Following the same procedure with the IPOS, Figure 4 is obtained, where the K_{pr} curve of each converter from Figure 3 is compared to a FPC. In first place, it is evident that the FPC always processes the 100% of the power that flows from the source to the load. However, PPC wise, it is observed that the ISOP and IPOS architectures achieve lower K_{pr} values when G_V gets closer to 1. This means that the closer V_{source} and V_{load} are between them, the lower power is processed by the converter. Comparing the curves achieved by the ISOP and the IPOS architectures, it is concluded that the ISOP obtains the lowest K_{pr} curve. Indeed, when G_V is lower than 0.5, the IPOS obtains absolute K_{pr} values higher than 1. This means that the IPOS converter is no longer working on the PPP range and all its benefits are lost.
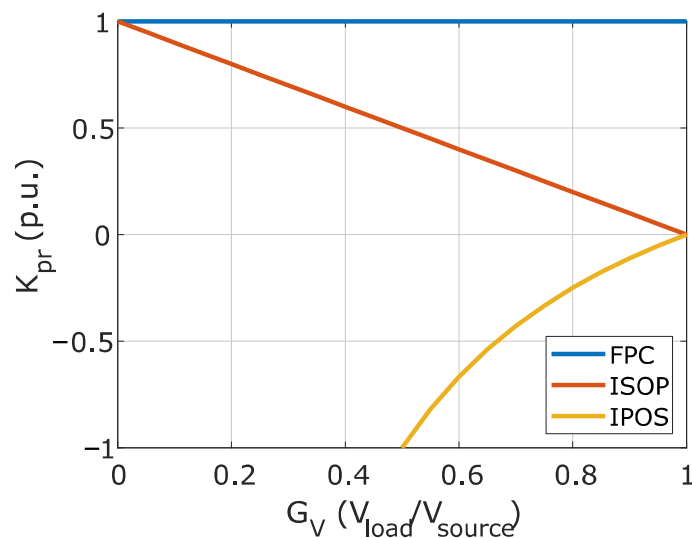

Figure 4. Processed power ratio of each converter from Figure 3.

3. Design of the PPP Based DC-DC Charging Unit

As shown in Figure 1, the concerned DC-DC converter is connected between a common DC bus and the ESS of the EV. This means that the application consists of a constant voltage source (DC bus) and a variable load (EV's ESS). When it comes to the DC bus, according to the SAE J1772 standard, its voltage value can vary from 200 V to 400 V in applications with power levels lower than 90 kW [4]. For this case, authors decided to stablish it at its maximum value, 400 V. On the other hand, ESS voltage wise, its value changes from one manufacturer to another, but, in most cases does not exceed 380 V [4]. Considering this, Figure 5 shows the stablished voltage and power curves for a hypothetical EV fast charging application. As it can be observed, it consists of an electric battery charging: constant current, up to 60% of state of charge (SOC), and constant voltage, up to an 80% of SOC.
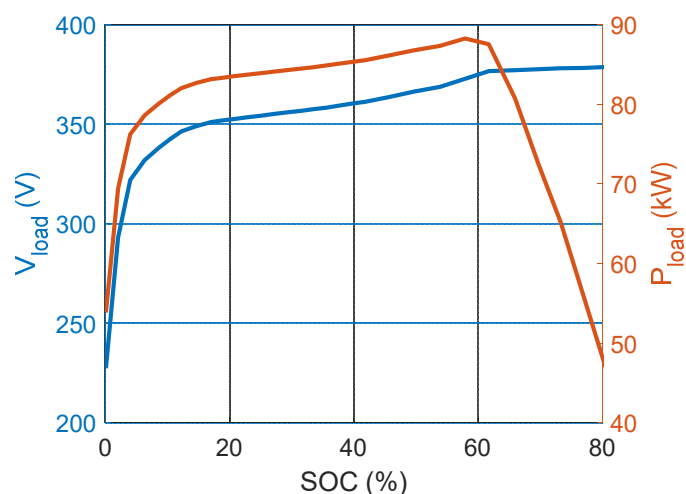
Figure 5. Voltage and power profile of the modeled ESS.

Bearing in mind that it consists of a voltage step-down application, according to Figure 4, the appropriate PPC architecture is the ISOP (Figure 3a). In addition, topology wise, a dual active bridge (DAB) is implemented for its simplicity and its bidirectional power flow (in case the application requires vehicle to grid functions). Figure 6 shows a high level schematic of the two solutions to compare: a DAB-FPP and a DAB-PPP.
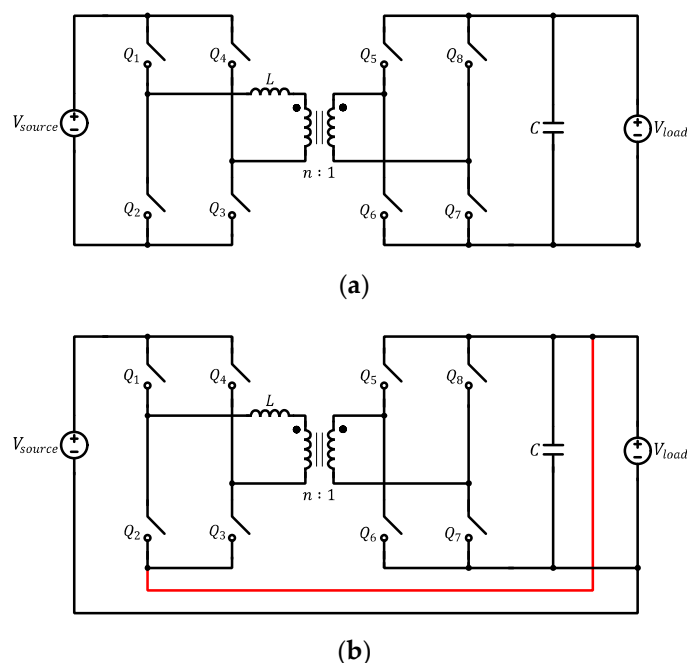

(**a**)

(**b**)

Figure 6. High level schematic of the selected solutions for the DC-DC charging unit. (**a**) DAB-FPP; (**b**) DAB-PPP.

Taking into account the voltage and power curves from Figure 5, Table 1 specifies the values of different electrical parameters related to the converter design. As it can be observed, voltage wise, both converters have the same output voltage. However, in case of the DAB-FPP the input voltage is constant, whereas, in the DAB-PPP consist of the difference between the source and the load. Then, when it comes to the K_{pr}, the DAB-PPP is expected to process just the 40% of the total power. Furthermore, this value is reduced to a 5% through the charging process. Next, since each converter has a different input-

output voltage relation, the required transformation ratio (n) and inductor (L) result in a different value.

Table 1. Main electrical parameters of the DAB-FPP and DAB-PPP.

Parameter	Value	
	DAB-FPP	**DAB-PPP**
V_{in} (V)	400	$173 \div 20$
V_{out} (V)	$227 \div 380$	$227 \div 380$
K_{pr} (p.u.)	1	$0.413 \div 0.05$
f_{sw} (kHz)	10	10
$\widetilde{P_{conv}}$ (kW)	90	23.25
n	1.0919	0.0919
L (µH)	23.05	1.94

Finally, before going into the simulation results, it is important to define the comparison parameters that will be used through the next subsections. In first place, there is the processed active power by the converter Equation (6), which has been already described.

$$K_{pr} = \frac{P_{conv}}{P_{sys}} \tag{6}$$

In second place, there is the non-active power processed by the converter. According to the definition given by IEEE [26], during the steady state of a DC-DC converter, the energy processed by storage components (capacitors and inductors) and that is not transferred from the source to the load is considered as non-active power flow (N), see Equations (7) and (8). In addition, due to the internally processed power by the converter, it is worth considering the non-active power flowing through the input source terminals of the converter Equation (9). Then, the total non-active power processed by the converter is calculated by summing the results obtained from Equations (7)–(9), see Equation (10).

$$N_L = \frac{2 \cdot \Delta E_L}{T_s} = \frac{2 \cdot \int_0^{D \cdot T_s} |v_L(t) \cdot i_L(t)| dt}{T_S} \tag{7}$$

$$N_C = \frac{2 \cdot \Delta E_C}{T_s} = \frac{2 \cdot \int_0^{D \cdot T_s} |v_C(t) \cdot i_C(t)| dt}{T_S} \tag{8}$$

$$N_{in} = \sqrt{S_{in}^2 - P_{in}^2} \tag{9}$$

$$N_{tot} = N_L + N_C + N_{in} \tag{10}$$

Last but not least, the efficiency of the converter and the efficiency of the system are calculated. When implementing FPP strategies, since the power processed by the converter is the same as the one that flows from the source to the load, η_{conv} and η_{sys} are the same Equation (11). However, PPP wise, the values of η_{conv} and η_{sys} are related by the K_{pr}, see Equation (12).

$$\eta_{sys_{FPP}} = \frac{V_{load}}{V_{source}} = \eta_{conv} = \frac{V_{out}}{V_{in}} \tag{11}$$

$$\eta_{sys_{PPP}} = 1 - K_{pr} \cdot (1 - \eta_{conv}) \tag{12}$$

4. Simulation Results

Once the case studio has been described, the next step is to simulate it and observe the obtained results. On the one hand, Figure 7 shows the processed active power ratio of each converter. As expected, the DAB-FPP always processes a 100% of the total power that flows from the source to the load, no matter the working point of the application.

However, the DAB-PPP achieves a reduction of the power processed by the converter, at least, up to a 40% of the total power. Furthermore, this value decreases as the ESS inside the EV charges, achieving a minimum value of 5%. This is due to the fact that as the ESS charges, its voltage value increases, provoking G_V to get closer to 1.
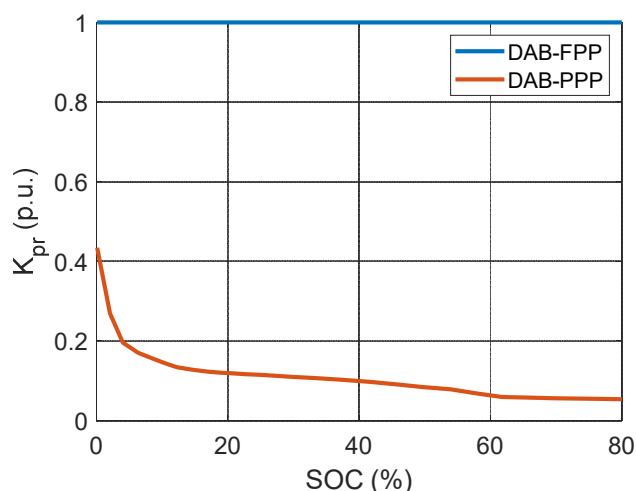

Figure 7. Processed power ratio comparison between the DAB-FPP and the DAB-PPP.

On the other hand, there is the non-active power. In this case, based on Equations (7)–(9), Figure 8 presents the different non-active power curves that exist inside the converter. As it can be observed, the most critical value in both solutions is the input non-active power, followed by the output capacitor. This is mainly due to the high RMS currents that exist in a DAB topology.
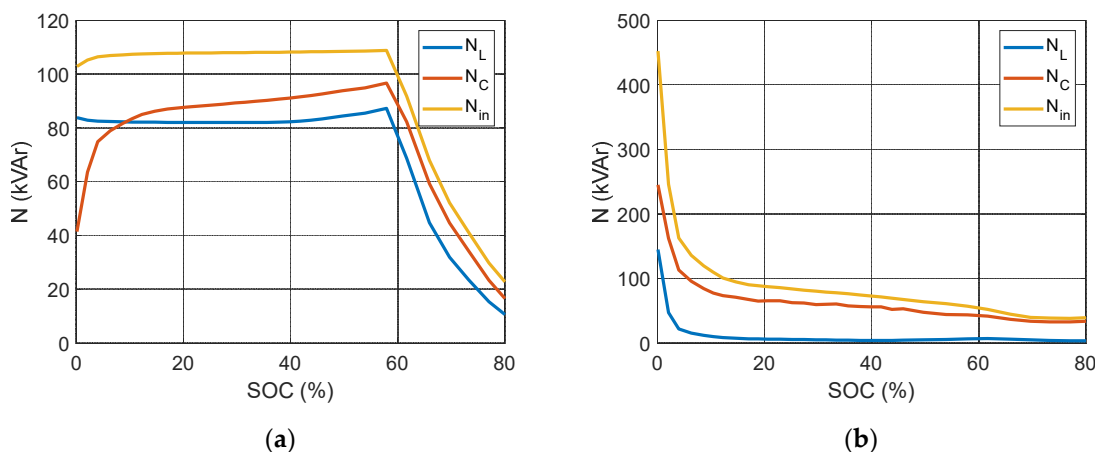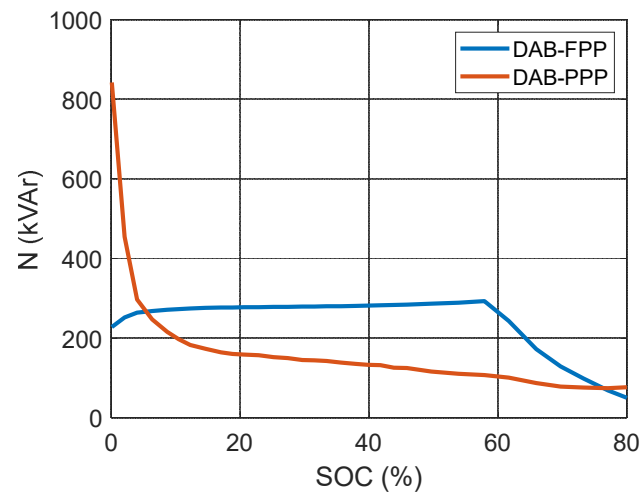

**Figure 8.** Processed non-active power by the components. (**a**) DAB-FPP; (**b**) DAB-PPP.

In order to have a better view of the non-active power results, Figure 9 shows the total non-active curves of each solution. Again, the DAB-PPP offers better results through great part of the charging process, except for the first charging periods (SOC < 5%), where the DAB-PPP processes higher amounts of non-active power. However, considering that the great majority of the EVs will reach the charging station with SOC values higher than a 5%, this period can be dismissed.

Figure 9. Processed non-active power comparison between the DAB-FPP and the DAB-PPP.

Finally, efficiency wise, Figure 10 shows that the DAB-PPP is a more efficient solution than the DAB-FPP. Similarly to Figure 9, at low SOC values, the DAB-PPP does not offer a good performance but, this quickly changes as the ESS of the EV charges and the K_{pr} decreases.
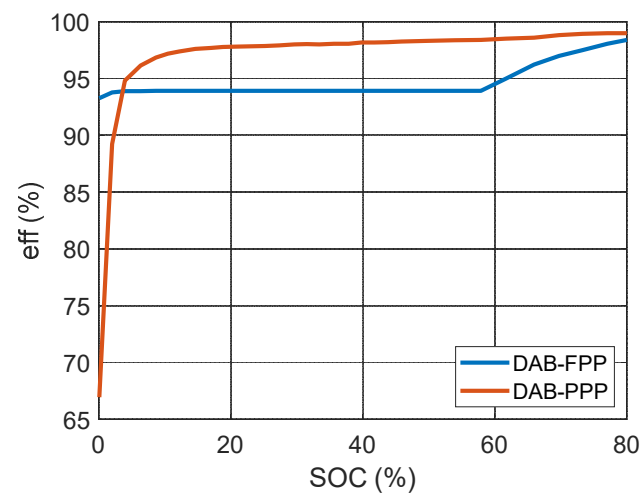

Figure 10. Efficiency comparison between the DAB-FPP and the DAB-PPP.

5. Experimental Platform

With the aim of confirming the benefits of implementing PPCs on EV fast charging applications, the present section details the experimental results obtained through the comparison between a DAB-FPP and a DAB-PPP.

5.1. Prototype Design

The experimental platform built for the concerned tests consists of a downscaled prototype whose voltage and power curves are shown in Figure 11. As it can be observed, it models the behavior of the charging process of an electric battery.
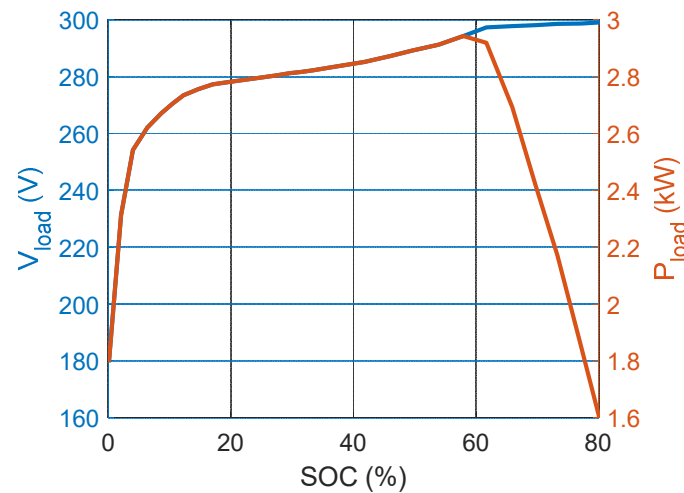
Figure 11. Modelled voltage and power profile of the load for the design of the prototype.

Based on the curves from Figure 11, Table 2 shows the main electrical design parameters of the experimental platform. There, it can be observed that it consists of a constant voltage source and a variable load. When it comes to the voltage values, 220 V has been decided to define as initial charging point. This way, it is assumed that the EV will arrive with at least a SOC of 1.5%.

Table 2. Main electrical parameters of the experimental platform.

Parameter	Value
$\widehat{P_{source}}$ (kW)	3
V_{source} (V)	320
V_{load} (V)	$220 \div 300$

Based on Figure 11 and bearing in mind the electrical parameters presented in Table 2, the main electrical parameters of the DAB-FPP and the DAB-PPP prototypes are obtained, see Table 3.

Table 3. Main electrical parameters of the DAB-FPP and DAB-PPP prototypes.

Parameter	Value	
	DAB-FPP	**DAB-PPP**
V_{in} (V)	320	$100 \div 20$
V_{out} (V)	$220 \div 300$	$220 \div 300$
K_{pr} (p.u.)	1	$0.31 \div 0.06$
f_{sw} (kHz)	50	50
$\widehat{P_{conv}}$ (kW)	3	0.69

Then, it is time to calculate the adequate design values for the components that exist inside the converter. In first place, there are the active components, which consist of 8 semiconductors: half of them located at the primary side of the transformer (Q_{1-4}) and the other half located at the secondary side of the transformer (Q_{5-8}). Bearing in mind Table 3, it can be concluded that switches Q_{5-8} must withstand at least 300V at both architectures. However, switches Q_{1-4} will observe different voltage values at the DAB-FPP and at the DAB-PPP, 320 V and 100 V respectively. Applying a security margin, it is decided to implement switches rated for the double of the voltage, see Table 4. As it can be observed, the same component is implemented for all the switches except for Q_{1-4} at the DAB-PPP. In consequence, the on resistance of the devices at its primary side is three times lower.

Table 4. Active and passive components of the DAB-FPP and DAB-PPP.

Component	Value	
	DAB-FPP	**DAB-PPP**
Q_{1-4}	IPT65R033G7 [1]	IPT111N20NFD [2]
Q_{5-8}	IPT65R033G7	IPT65R033G7
C (μF)	MKP1848C [3]	MKP1848C
n	1.31	0.261
L (μH)	101.5	305.34 [4]

[1] $V_{DS} = 650$ V, $I_D = 69$ A, $R_{DS} = 33$ mΩ. [2] $V_{DS} = 250$ V, $I_D = 96$ A, $R_{DS} = 11.1$ mΩ. [3] VISHAY 500 V 100 μF (2 times paralleled). [4] The inductance is located at the secondary side of the transformer.

On the other hand, when it comes to the transformation ratio (taking as example the DAB-FPP), its value has been designed for an intermediate value between two extreme working conditions: starting the battery charge Equation (13) and ending the battery charge Equation (14). The obtained value is shown in Equation (15).

$$n_1 = \frac{V_{in}}{V_{out}} = \frac{100}{220} = 0.\widehat{45} \tag{13}$$

$$n_2 = \frac{V_{in}}{V_{out}} = \frac{20}{300} = 0.0\widehat{6} \tag{14}$$

$$n_{DAB,PPP} = \frac{0.\widehat{45} + 0.0\widehat{6}}{2} = 0.261 \tag{15}$$

Once the transformation ratio is defined, inductor's value must be designed for the most critical point. In this case, the moment in which the converter processes more power is at the start of the charge. Equation (16) shows the obtained inductance refereed to primary side.

$$L' \leq \frac{n \cdot V_{in} \cdot V_{out}}{8 \cdot f_{sw} \cdot P_{conv}} = \frac{0.261 \times 100 \times 220}{8 \times 50 \times 10^3 \times 690} = 20.8 \text{ μH} \tag{16}$$

In order to reduce the current through the inductor, it is decided to locate it at the secondary side of the transformer Equation (17).

$$L = \frac{L'}{n^2} = \frac{20.8 \times 10^{-6}}{0.261^2} = 305.33 \text{ μH} \tag{17}$$

Finally, the two prototypes to compare are shown in Figure 12. As it can be observed, the most apparent difference between them are the magnetics. To be more precise, the nucleus used for the DAB-FPP is a PM8770 type, whereas, the one used for the DAB-PPP is a PM6249. This supposes a 65% reduction in the volume of the magnetics. In relation to the transformer and the inductor, all of them are assembled at the laboratory.
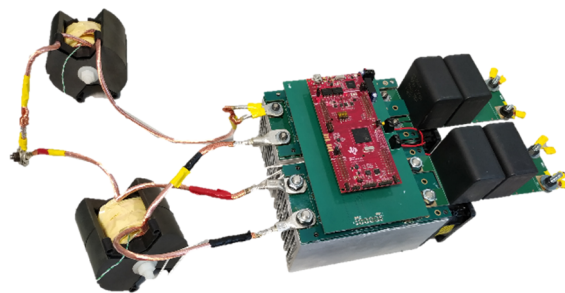
(**a**)
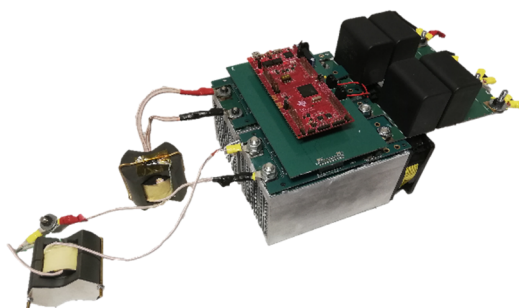
(**b**)

Figure 12. Experimental prototype. (**a**) DAB-FPP; (**b**) DAB-PPP.

5.2. Test Conditions

Once the entire prototype has been described, the next step is to test it. For this purpose, the power converter is forced to work at four different points, see Table 5. These points model the charging process of the battery and they have been extracted from Figure 11. As it can be observed, the source voltage always remains constant and the load voltage increases together with the power. The final point corresponds to the constant voltage period, where, the power consumed by the load decreases. In this case, the selected value is around a 50% of the nominal power.

Table 5. Testing conditions extracted from Figure 11.

SOC (%)	V_{source} (V)	V_{load} (V)	P_{load} (kW)
1.5	320	220	2.2
5.7	320	260	2.6
60	320	300	3
80	320	300	1.5

On the other hand, when it comes to the experimental set up, Figure 13a,b show a simplified electric diagram of the implemented set-ups for the DAB-FPP and the DAB-PPP, respectively. As it can be observed, in the case of the DAB-FPP, 4 parameters are measured (I_{source}, I_{load}, V_{source} and V_{load}). However, DAB-PPP wise, 6 different parameters are required (I_{source}, I_{load}, I_{out}, V_{source}, V_{in} and V_{out}).
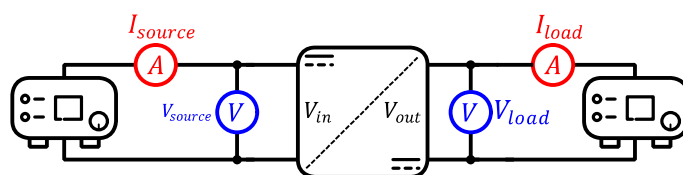

(**a**)
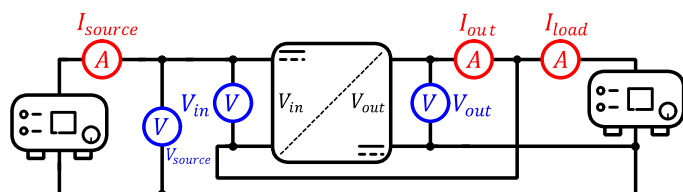
(**b**)

Figure 13. Simplified electric circuit of the experimental set-up. (**a**) DAB-FPP; (**b**) DAB-PPP.

Then, with the aim of securing that the semiconductors do not exceed the temperature limit, a thermocouple is stuck to the PCB and to one of the semiconductors of each

full-bridge. Finally, Figure 14 shows a real image of the set-up used for the experimental tests. More detailed information about the equipment used through the test is given in Appendix A.
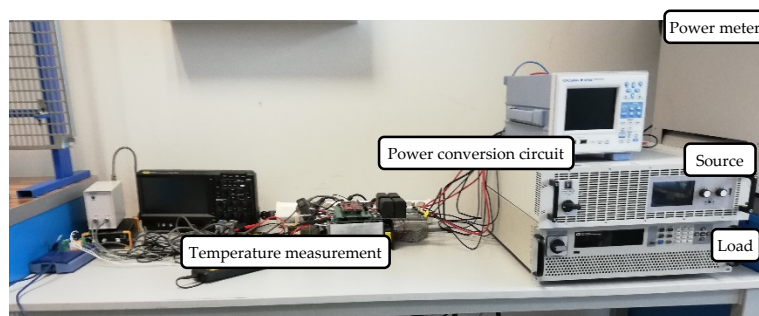

Figure 14. The built set-up for the experimental tests.

5.3. Experimental Results

Once the test conditions have been correctly defined, the next step is to observe the obtained results. Following the testing points defined in Table 5, Figure 15 shows the temperature evolution of the semiconductors and the PCBs. It is worth mentioning that each dark dot marks the beginning of a new testing point and that, since the power block has been oversized, the obtained temperature values are not disturbing.

On the one hand, Figure 15a shows the temperature results obtained by the DAB-FPP. There, it can be observed that the most critical component is the secondary side semiconductor, which achieves a maximum temperature of 32.4 °C when working at maximum power point (V_{load} = 300 V & SOC = 60%). On the other hand, Figure 15b shows the results obtained by the DAB-PPP. In this case, the most critical component is the primary side semiconductor, which achieves a maximum temperature of 29 °C when working at the initial charging point (V_{load} = 220 V). Then, as the load voltage increases, the temperature of the concerned component decreases. This thermal behavior is completely different to the one obtained by the DAB-FPP but, it can be very interesting to take it into account when designing a PPC. Indeed, assuming that the initial charging conditions vary in voltage rapidly, see Figure 11, the engineers can optimize the designing criteria by expecting a lower thermal stress.
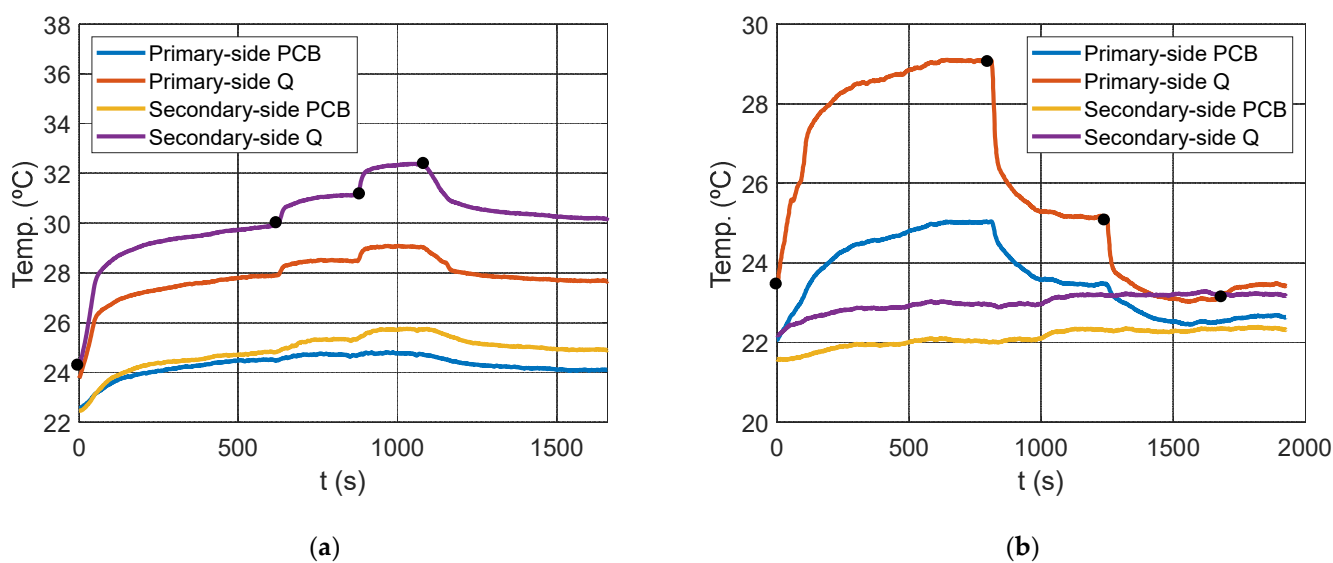

Figure 15. Temperature evolution. (**a**) DAB-FPP; (**b**) DAB-PPP.

The fact that the temperature of the component decreases as the battery charges is directly related to the K_{pr}. This is proved in Table 6, where the system and converter powers are shown for each testing point. Analyzing the DAB-PPP column, it is observed that P_{source} increases through the first three working points (constant current mode) and, in the last one, it decreases (constant voltage mode). However, when it comes to the input power (P_{in}) of the converter, it always decreases in value. This is due to the fact that, as the battery charges, V_{load} is getting closer to V_{source}, causing a reduction in K_{pr}. At the last point, the K_{pr} is not reduced because V_{load} is maintained at 300 V.

Table 6. Processed power by the DAB-FPP and DAB-PPP.

Test Condition	Parameter	Value	
		DAB-FPP	DAB-PPP
$V_{load} = 220$ (V)	P_{source} (kW)	2.21	2.24
	P_{in} (kW)		0.699
	K_{pr} (p.u.)	1	0.312
$V_{load} = 260$ (V)	P_{source} (kW)	2.58	2.53
	P_{in} (kW)		0.474
	K_{pr} (p.u.)	1	0.187
$V_{load} = 300$ (V) SOC = 60%	P_{source} (kW)	3.02	2.85
	P_{in} (kW)		0.176
	K_{pr} (p.u.)	1	0.062
$V_{load} = 300$ (V) SOC = 80%	P_{source} (kW)	1.54	1.38
	P_{in} (kW)		0.086
	K_{pr} (p.u.)	1	0.062

Efficiency wise, Figure 16 shows the obtained results. As it can be observed, although the efficiency of the DAB-PPP converter is not extraordinary (most of the cases bellow the DAB-FPP), the efficiency of the DAB-PPP system achieves the best results, with a peak value of 99.62%. Compared to the maximum efficiency obtained by the DAB-FPP (94.7%), it can be concluded that the DAB-PPP offers a much efficient performance.
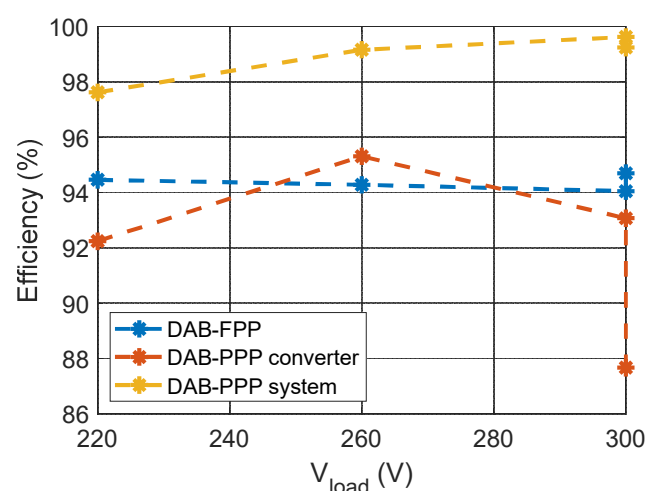
Figure 16. Efficiency obtained by the prototypes.

6. Conclusions

The present paper compares, in terms of processed power by the converter and efficiency, the performance between a DAB-FPP and a DAB-PPP for an EV fast charging application. Through the simulations, it is observed that the DAB-PPP reduces the active

and non-active power to process by the converter and that it improves the efficiency. This is confirmed by testing two downscaled prototypes. On the one hand, regarding the temperature obtained by the most critical component, it is concluded that the DAB-PPP achieves lower temperature stress. On the other hand, processed power wise, it is observed that the DAB-PPP processes between a 30 and a 6% of the total power that flows from the source to the load. In consequence, the achieved efficiencies always improve the ones obtained by the DAB-FPP. Apart from that, when it comes to the size of the magnetics (inductor and transformer), it is observed that a volume reduction of 65% is achieved with the DAB-PPP. To sum up, in case the regulation of the country does not oblige to implement galvanic isolation at the charging unit, PPCs turn to be more efficient and lower size solutions than conventional FPP converters.

7. Future Lines

With the aim of improving the present paper, the authors propose the next future lines are:

- Include a processed non-active power analysis on the prototypes that verifies the reduction of energy processed by storage elements.
- As observed in Figures 9 and 10, the DAB-PPP presents higher processed non-active power and lower efficiency at initial charging periods. This is due to the fact that power converters inside PPC architectures are required to work at a wider operation range than FPCs [20]. In consequence, lower performance is achieved at extreme working points. In order to improve this, extended analysis on advanced modulation methods is proposed.
- Although the main objective of the paper is to compare the behavior of a given topology (in this case a DAB) when it is implemented on a FPP architecture and on a PPP architecture, this comparison may not be considered completely fair, since one of the solutions provides galvanic isolation and the other one does not. Therefore, it is proposed to extend the comparison by adding the AC-DC stage. Indeed, as shown in Figure 1, every EV fast charging station consists of an AC-DC and a DC-DC stage and, when it comes to the galvanic isolation, it can be located at one stage or the other. This way, the galvanic isolation can be provided by both solutions: non-isolated AC-DC stage with an isolated DC-DC stage (DAB-FPP) and an isolated AC-DC stage with a non-isolated DC-DC stage (DAB-PPP).

Author Contributions: Conceptualization, J.A. and I.A.; validation, J.A., A.A.; investigation, J.A.; data curation, J.A.; writing—original draft preparation, J.A.; writing—review and editing, J.A., I.A. and A.A.; supervision, I.A.; All authors have read and agreed to the published version of the manuscript.

Appendix A

The objective of the present appendix is to list the equipment that has been used for the correct measuring of the experimental tests, see Table A1.

Table A1. Equipment used for the measuring of the experimental tests.

Description	Reference
Source	ITECH IT6012C-800-40
Load	EA-ELR 9750-22
Power meter	YOKOGAWA WT500
Temperature measurement	Pico TC-08

References

1. Irle, R. EV-Volumes—The Electric Vehicle World Sales Database. 2018. Available online: http://www.ev-volumes.com/ (accessed on 6 March 2019).
2. Gorzelany, J. The Longest Range Electric Cars For. 2019. Available online: https://insideevs.com/features/342424/the-longest-range-electric-cars-for-2019/ (accessed on 6 March 2019).
3. Dickerman, L.; Harrison, J. A new car, a new grid: The electric car is back (with Help from New Batteries, a Smarter Grid, and Uncle Sam). *IEEE Power Energy Mag.* **2010**, *8*, 55–61.
4. Christen, D. Analysis and Performance Evaluation of Converter Systems for EV-Ultra-Fast Charging Stations with Integrated Grid Storage. Doctoral Dissertation, ETH Zurich, Zürich, Switzerland, 2017; p. 195.
5. Etter Place: What Went Wrong for the Electric car Startup? | Environment | The Guardian. Available online: https://www.theguardian.com/environment/2013/mar/05/better-place-wrong-electric-car-startup (accessed on 23 September 2020).
6. Bosshard, R.; Badstubner, U.; Kolar, J.W.; Stevanovic, I. Comparative evaluation of control methods for Inductive Power Transfer. In Proceedings of the 2012 International Conference on Renewable Energy Research and Applications (ICRERA), Nagasaki, Japan, 11–14 November 2012.
7. Chargemap—Electric Cars' Charging Station Map. Available online: https://chargemap.com/map (accessed on 23 September 2020).
8. Iyer, V.M.; Gulur, S.; Gohil, G.; Bhattacharya, S. Extreme fast charging station architecture for electric vehicles with partial power processing. In Proceedings of the 2018 IEEE Applied Power Electronics Conference and Exposition (APEC), San Antonio, TX, USA, 4–8 March 2018; pp. 659–665.
9. Zapata, J.W.; Kouro, S.; Carrasco, G.; Meynard, T.A. Step-down partial power DC-DC converters for two-stage photovoltaic string inverters. *Electronics* **2019**, *8*, 87.
10. Zapata, J.W.; Kouro, S.; Carrasco, G.; Renaudineau, H. Step-up partial power DC-DC converters for two-stage PV systems with interleaved current performance. *Energies* **2018**, *11*, 357.
11. Zientarski, J.R.R.; Martins, M.L.d.; Pinheiro, J.R.; Hey, H.L. Series-Connected Partial-Power Converters Applied to PV Systems: A Design Approach Based on Step-Up/Down Voltage Regulation Range. *IEEE Trans. Power Electron.* **2017**, *33*, 7622–7633.
12. Mira, M.C.; Zhang, Z.; Jorgensen, K.L.; Andersen, M.A.E. Fractional Charging Converter with High Efficiency and Low Cost for Electrochemical Energy Storage Devices. *IEEE Trans. Ind. Appl.* **2019**, *55*, 7461–7470.
13. Mishra, S.; Tamballa, S.; Pallantala, M.; Raju, S.; Mohan, N. Cascaded Dual-Active Bridge Cell Based Partial Power Converter for Battery Emulation. In Proceedings of the 2019 20th Workshop on Control and Modeling for Power Electronics (COMPEL), Toronto, ON, Canada, 17–20 June 2019; pp. 1–7.
14. Pape, M.; Kazerani, M. Turbine Startup and Shutdown in Wind Farms Featuring Partial Power Processing Converters. *IEEE Open Access J. Power Energy* **2020**, *7*, 254–264.
15. Pape, M.; Kazerani, M. An Offshore Wind Farm with DC Collection System Featuring Differential Power Processing. *IEEE Trans. Energy Convers.* **2019**, *35*, 222–236.
16. Qin, S.; Barth, C.B.; Pilawa-Podgurski, R.C.N. Enhancing Microinverter Energy Capture with Submodule Differential Power Processing. *IEEE Trans. Power Electron.* **2014**, *31*, 3575–3585.
17. Kasper, M.; Bortis, D.; Kolar, J.W. Unified power flow analysis of string current diverters. *Electr. Eng.* **2018**, *100*, 2085–2094.
18. Iyer, V.M.; Gulur, S.; Bhattacharya, S.; Ramabhadran, R. A Partial Power Converter Interface for Battery Energy Storage Integration with a DC Microgrid. In Proceedings of the 2019 IEEE Energy Conversion Congress and Exposition (ECCE), Baltimore, MD, USA, 29 September–3 October 2019; pp. 5783–5790.
19. Candan, E.; Shenoy, P.S.; Pilawa-Podgurski, R.C.N. A Series-Stacked Power Delivery Architecture with Isolated Converters For Energy Efficient Data Centers. *IEEE Trans. Power Electron.* **2014**, *31*, 3690–3703.
20. Iyer, V.M.; Gulur, S.; Gohil, G.; Bhattacharya, S. An Approach towards Extreme Fast Charging Station Power Delivery for Electric Vehicles with Partial Power Processing. *IEEE Trans. Ind. Electron.* **2019**, *67*, 8076–8808.
21. Rojas, J.; Renaudineau, H.; Kouro, S.; Rivera, S. Partial power DC-DC converter for electric vehicle fast charging stations. In Proceedings of the IECON 2017-43rd Annual Conference of the IEEE Industrial Electronics Society, Beijing, China, 29 October–1 November 2017; Volume 2017, pp. 5274–5279.
22. Buck, J. International electrotechnical commission. *Handb. Transnatl. Econ. Gov. Regimes* **2016**, 573–584, doi:10.1163/EJ.9789004163300.I-1081.494.
23. Anzola, J.; Aizpuru, I.; Romero, A.A.; Loiti, A.A.; Lopez-Erauskin, R.; Artal-Sevil, J.S.; Bernal, C. Review of Architectures Based on Partial Power Processing for DC-DC Applications. *IEEE Access* **2020**, *8*, 103405–103418.
24. Zhao, J.; Yeates, K.; Han, Y. Analysis of High Efficiency DC/DC Converter Processing Partial Input/Output Power. In Proceedings of the 2013 IEEE 14th Workshop on Control and Modeling for Power Electronics (COMPEL), Salt Lake City, UT, USA, 23–26 June 2013; pp. 1–8.

25. Chen, L.; Wu, H.; Xu, P.; Hu, H.; Wan, C. A high step-down non-isolated bus converter with partial power conversion based on synchronous LLC resonant converter. In Proceedings of the 2015 IEEE Applied Power Electronics Conference and Exposition (APEC), Charlotte, NC, USA, 15–19 March 2015; Volume 2015, pp. 1950–1955.

26. IEEE. IEEE Standard Definitions for the Measurements of Electric Power Quantities Under Sinusoidal, Nonsinusoidal, Balanced or Unbalanced Conditions. Available online: https://pdfs.semanticscholar.org/29a9/36f02016a71ca26ea5d4fa05a2a974984b14.pdf?_ga=2.41965094.2034374545.1611191539-1641229895.1606892986 (accessed on 8 April 2019).